MIT Libraries | DSpace@MIT

MIT Open Access Articles

Polymethyl methacrylate/hydrogen silsesquioxane bilayer resist electron beam lithography process for etching 25 nm wide magnetic wires

The MIT Faculty has made this article openly available. ***Please share*** how this access benefits you. Your story matters.

Citation: Currivan, Jean Anne, Saima Siddiqui, Sungmin Ahn, Larysa Tryputen, Geoffrey S. D. Beach, Marc A. Baldo, and Caroline A. Ross. "Polymethyl Methacrylate/hydrogen Silsesquioxane Bilayer Resist Electron Beam Lithography Process for Etching 25 Nm Wide Magnetic Wires." J. Vac. Sci. Technol. B 32, no. 2 (March 2014): 021601. © 2014 American Vacuum Society.

As Published: http://dx.doi.org/10.1116/1.4867753

Publisher: American Institute of Physics

Persistent URL: http://hdl.handle.net/1721.1/91649

Version: Final published version: final published article, as it appeared in a journal, conference proceedings, or other formally published context

Terms of Use: Article is made available in accordance with the publisher's policy and may be subject to US copyright law. Please refer to the publisher's site for terms of use.

Massachusetts Institute of Technology

Polymethyl methacrylate/hydrogen silsesquioxane bilayer resist electron beam lithography process for etching 25 nm wide magnetic wires

Jean Anne Currivan[a)]
Department of Electrical Engineering and Computer Science, Massachusetts Institute of Technology, Cambridge, Massachusetts 02139 and Department Of Physics, Harvard University, Cambridge, Massachusetts 02138

Saima Siddiqui
Department of Electrical Engineering and Computer Science, Massachusetts Institute of Technology, Cambridge, Massachusetts 02139

Sungmin Ahn, Larysa Tryputen, and Geoffrey S. D. Beach
Department of Materials Science and Engineering, Massachusetts Institute of Technology, Cambridge, Massachusetts 02139

Marc A. Baldo
Department of Electrical Engineering and Computer Science, Massachusetts Institute of Technology, Cambridge, Massachusetts 02139

Caroline A. Ross
Department of Materials Science and Engineering, Massachusetts Institute of Technology, Cambridge, Massachusetts 02139

(Received 21 January 2014; accepted 21 February 2014; published 7 March 2014)

A method of patterning magnetic metallic thin films is presented using a bilayer polymethyl methacrylate and hydrogen silsesquioxane electron beam lithography resist mask combined with ion beam etching. The bilayer resist process allows for the combination of a high-resolution resist mask with easy postprocess removal of the mask without damage to the magnetic quality of the film. $Co_{60}Fe_{20}B_{20}$ and Co/Ni multilayer films were patterned with electron beam lithography at 10–125 keV down to 25 nm wide features with 2 nm average root-mean square edge roughness. Both the in-plane and out-of-plane magnetic anisotropies of the respective film types were preserved after patterning. © *2014 American Vacuum Society*. [http://dx.doi.org/10.1116/1.4867753]

I. INTRODUCTION

There is great excitement in developing energy-efficient nonvolatile magnetic memory and logic devices[1,2] based on the movement of domain walls in magnetic wires or the reversal of magnetic nanostructures. Patterning of thin films into sub-100 nm features is essential so that these magnetic devices can have switching energies competitive with those of CMOS-based devices.[3] In particular, low edge roughness is required for reproducibility of the magnetic switching characteristics, since edge roughness in the nanostructures can act as a domain wall trap, increasing the energy required to translate a domain wall through the material, or can promote the formation of reverse domains.[4–6]

Here, we describe a method for patterning metallic wires down to 25 nm width using a removable bilayer polymethyl methacrylate (PMMA) and hydrogen silsesquioxane (HSQ) resist mask combined with ion beam etching. A PMMA/HSQ bilayer has been investigated previously for liftoff processes[7,8] but not as a mask for subtractive patterning. The bilayer process described here was developed to facilitate patterning of transition metal alloy films, with $Co_{60}Fe_{20}B_{20}$ (CoFeB) chosen as a primary example. CoFeB is a soft ferromagnet that has been incorporated into high performance magnetic tunnel junctions, making it an ideal candidate for magnetic memory and logic.[9] However, reactive ion etching of transition metals and their alloys is difficult since they form involatile halides when treated with many common reactive etching gases.[10] Thus, high-resolution subtractive patterning is usually done using ion beam etching (ion milling), focused ion beam patterning, or damascene processes to selectively remove the metal.[11–13]

HSQ is an excellent negative-tone resist for high-resolution electron beam lithography down to 4.5 nm half-pitch.[14,15] However, after exposure and development, the etch resistance of crosslinked HSQ increases,[8] and its subsequent removal requires a hydrofluoric acid dip or a CF_4 reactive ion etch (RIE); both can damage an underlying metallic thin film. This motivated our development of a bilayer resist process which combines the high etch resistance of HSQ with an underlying PMMA layer that allows removal of the HSQ features using a solvent such as n-methyl-2-pyrrolidone (NMP) or acetone, after etching the metal film. We show that this method can produce magnetic wires with widths down to 25 and 2 nm average edge roughness.

II. EXPERIMENTAL METHODS

Figure 1(a) shows the process flow for patterning the magnetic structures. All patterning was done on silicon substrates with a native oxide. In step 1, amorphous Ta 3/CoFeB 10/Au 3 (where the numbers represent thicknesses in nanometer) films were deposited using UHV DC

a)Author to whom correspondence should be addressed; electronic mail: currivan@mit.edu

 2166-2746/2014/32(2)/021601/5/$30.00 © 2014 American Vacuum Society

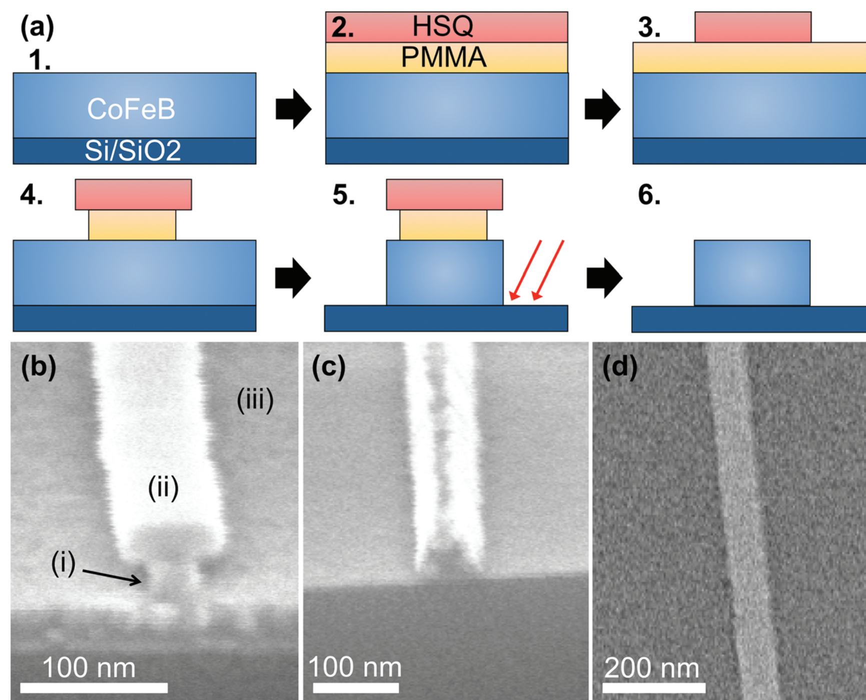

FIG. 1. (Color) (a) Schematic illustration of the step-by-step fabrication process. (b) Cross-sectional SEM image after step 4 showing the bilayer resist on top of the CoFeB thin film. (i) is PMMA, (ii) is HSQ, and (iii) is CoFeB. (c) After ion beam etching to transfer the feature into the metal (step 5). (d) SEM image of resulting 71 nm wide CoFeB wire (step 6).

magnetron sputter deposition at 2×10^{-8} Torr. Ta 5/Cu 8/Co 0.3/[Ni 0.9/Co 0.3] $\times$ 4/NiFe 2/Ta 5 was also deposited on a thermally oxidized Si substrate using confocal magnetron sputtering to provide an example of a film with perpendicular magnetic anisotropy, with four repeats of the Ni/Co multilayer (for the details of film preparation and magnetic properties, see Ref. 16). In step 2, 2% PMMA in anisole was spun at 4 krpm for 60 s and baked at 180 °C for 90 s to produce a film thickness of 30 nm. Then 2% HSQ in methyl isobutyl ketone was spun at 4 krpm for 60 s and baked at 110 °C for 60 s to produce a film thickness of 30 nm. In step 3, the HSQ was exposed. For line widths >50 nm, a Raith 150 electron beam lithography tool was used at 30 keV electron energy and 400–800 μC/cm^2 dose. The samples were developed using 2.4% tetramethylammonium hydroxide in water (CD-26) developer for 2–4 min. For <50 nm line width, an Elionix F-125 electron beam lithography tool was used at 125 keV with dose 32 mC/cm^2 and developed using 4% NaCl/1% NaOH in water for 20 s. The electron beam exposure of the HSQ caused scission in the PMMA beneath the HSQ, which increased its solubility, so HSQ development had to be carried out using nonsolvents for PMMA.

In step 4, an O_2 RIE was performed at base pressure 1×10^{-5} Torr, using 10 sccm oxygen and 90 W, for 60–180 s. The etch time was chosen to produce an undercut of the PMMA under the HSQ. In step 5, ion beam etching was used to transfer the pattern into the CoFeB using Ar ions at base pressure 1×10^{-7} Torr, with Ar flow of 1.5 sccm, 10 mA beam current, and a 2 cm beam diameter. In step 6, the PMMA/HSQ mask was removed by placing the sample in NMP at 135 °C for 90 min, sonicating for 30 min, leaving the sample in NMP for 15 h unheated, then sonicating again for 30 min. This dissolved the PMMA and removed the HSQ. The extended removal time is required due to redeposition of the HSQ on the sidewalls of the structures during ion milling, which reduced the surface area of PMMA exposed to the solvent.

III. RESULTS AND DISCUSSION

Figure 1 shows scanning electron microscope (SEM) images during different steps of the process. Figure 1(b) shows a cross section of the double-resist stack after step 4, where (i) is PMMA, (ii) is HSQ, and (iii) is the CoFeB thin film. The HSQ line was nominally 75 nm wide, with an actual average width of $w_{HSQ} = 71$ nm (to within ±5%, from the SEM images); the PMMA had $w_{PMMA} = 33$ nm. The HSQ was 30 nm thick, with 28 nm thick PMMA underneath. We ensured the HSQ thickness was thicker than the 16 nm thick film, since the ion beam etch rate was found to be similar for HSQ and the metallic film. The O_2 RIE process time of 120 s was chosen to produce an undercut in the PMMA so that the high-resolution HSQ mask defined the eventual feature size in the metal.

Figure 1(c) shows the sample after step 5 with $w = 71$ nm at the base of the feature. The mask shows a tapered cross section after ion beam etching. Figure 1(d) shows a top–down view of the CoFeB wire after step 6 with $w = 71$ nm, matching the width of the HSQ mask.

Figure 2 demonstrates the effects of the linewidth on the undercut of the PMMA. The bilayer resist in this example was made from higher concentration solutions of 4% PMMA in anisole and 4% HSQ in methyl isobutyl ketone keeping all other parameters the same as above to improve

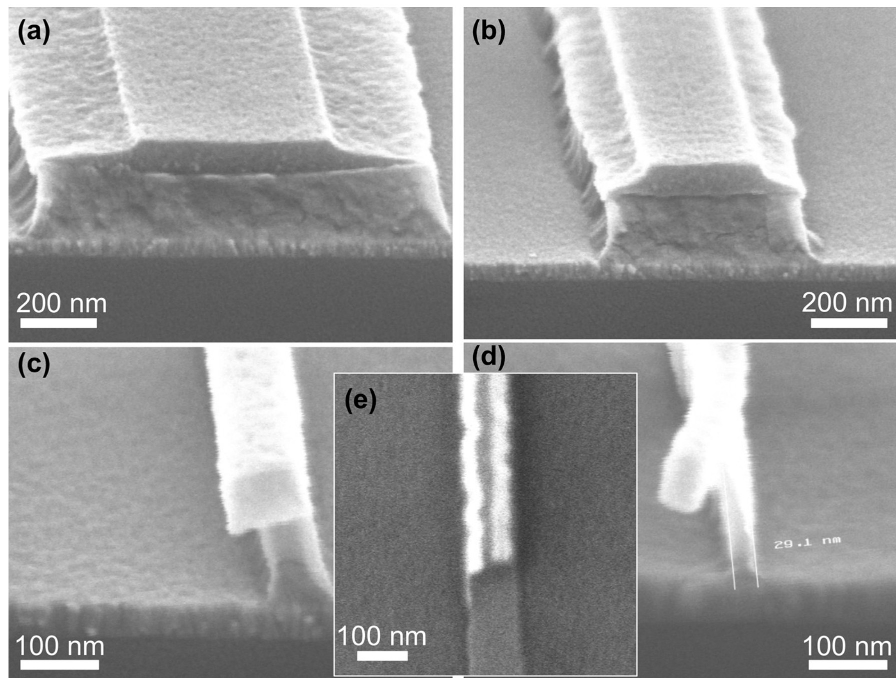

FIG. 2. Cross-sectional SEM images of bilayer resist stack after 1 min O_2 RIE (step 4), for HSQ widths (a) 468 nm, (b) 261 nm, (c) 95 nm, and (d) 61 nm. This RIE time was not long enough for the wider two HSQ masks and did not produce an undercut. (e) SEM image of metal wire showing only partial mask removal due to nonoptimized RIE time.

visibility of the stack during SEM. The HSQ was exposed at 10 keV and developed to form lines with w_{HSQ} = (a) 468 nm, (b) 261 nm, (c) 95 nm, and (d) 61 nm (±5%) followed by step 4 O_2 RIE for 60 s. The HSQ is slightly tapered in (a) and (b), which could be due to backscattered electron exposure. The SEM images show that while this RIE time produced an undercut of PMMA for $w_{HSQ} < 100$ nm in (c) and (d), it was insufficient to produce an undercut in the wider lines of (a) and (b), i.e., the O_2 RIE time must be matched to the desired wire width. The linewidth dependence of the PMMA undercut may originate from differences in the electron beam exposure of the PMMA affecting its response to the oxygen RIE. Figure 2(e) shows a top–down SEM image of a metal wire after ion beam etching for a case where the

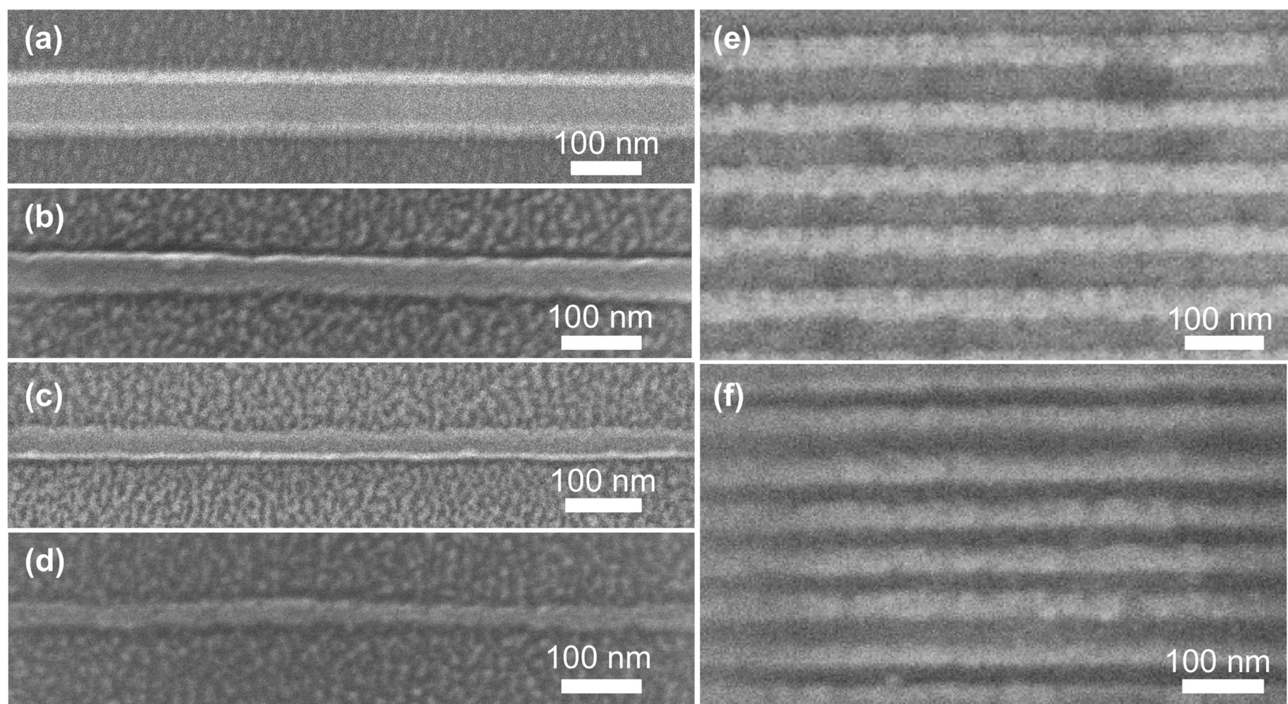

FIG. 3. (a)–(d) HIM images of CoFeB nanowires of average width w = (a) 89 nm, (b) 46 nm, (c) 39 nm, and (d) 24 nm. (e)–(f) Helium-ion images of wire arrays with (e) pitch 76 nm, w = 30 nm and (f) pitch 26 nm, w = 26 nm.

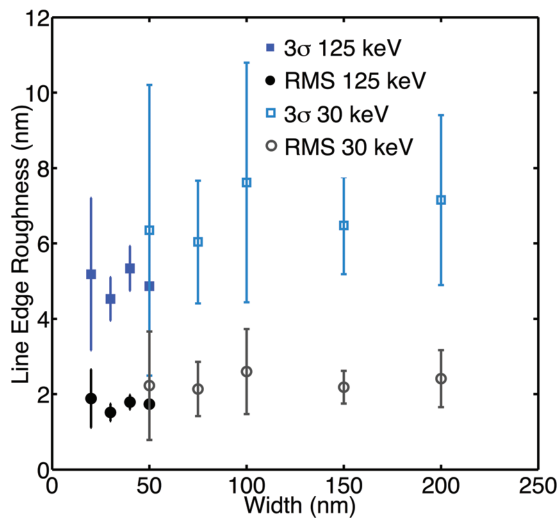

FIG. 4. (Color) Average LER vs wire width. The standard deviation is measured across five separate wires on the same substrate. Dark blue, closed square points are 3σ LER at 125 keV lithography electron beam voltage used for narrower lines; black, closed circle points are RMS LER at 125 keV. Light blue, open square points are 3σ LER at 30 keV used for wider lines; gray, open circle points are RMS LER at 30 keV.

RIE time was optimized for wires narrower than 100 nm. A remaining part of the mask can be seen on the metal wire in the upper part of the image.

Images from a helium-ion microscope (HIM) of metal wires made using the bilayer resist etching process are shown in Fig. 3. Isolated CoFeB wires of average $w=$ (a) 89 nm, (b) 46 nm, (c) 39 nm, and (d) 24 nm were obtained with complete removal of the bilayer mask after ion beam etching. These widths matched the HSQ mask widths.

Figures 3(e) and 3(f) show closely spaced arrays of patterned lines. The lines were exposed with a 125 keV electron beam and area dose 6.4 mC/cm^2. This dose is lower than that used for isolated lines (32 mC/cm^2) due to proximity effects of the nearby lines. The proximity effect was similar to that of a single layer of HSQ, since only the HSQ is developed and not the PMMA. Figure 3(e) shows a HIM image of CoFeB lines with average $w=30$ nm and pitch $p=76$ nm, and (f) $w=26$ nm and $p=26$ nm. Below this pitch, the lines were not resolved for these exposure and development conditions. The root-mean square (RMS) line edge roughness (LER) of these lines, calculated as described below, was $r_{RMS}=2.7$ nm for (e) and $r_{RMS}=1.97$ nm for (f), which is similar to those of isolated lines of same width. We conclude that the proximity of multiple lines does not affect the LER of small-pitched CoFeB lines patterned using this method.

Figure 4 describes the 3σ and RMS LER r versus wire width w. For each nominal w, five SEM images (pixel size 0.89 nm) were taken of different wires patterned on the same substrate. Both the average and standard deviation of r were then calculated by measuring the edge deviation in nanometer along the wire using SUMMIT Litho Analysis Software.[17] We find $r_{RMS}\cong 2$ nm independent of wire width. These wires were up to 1 mm long, and the r_{RMS} was the same at several different locations measured along the length. The LER of the patterned HSQ layer was 0.6–0.7 nm, so there was an increase of 1.3–1.4 nm in LER when the pattern was transferred from the HSQ to the metal by ion beam etching. The electron beam voltage was increased from 30 to 125 keV for wires <50 nm to reduce the electron beam diameter.

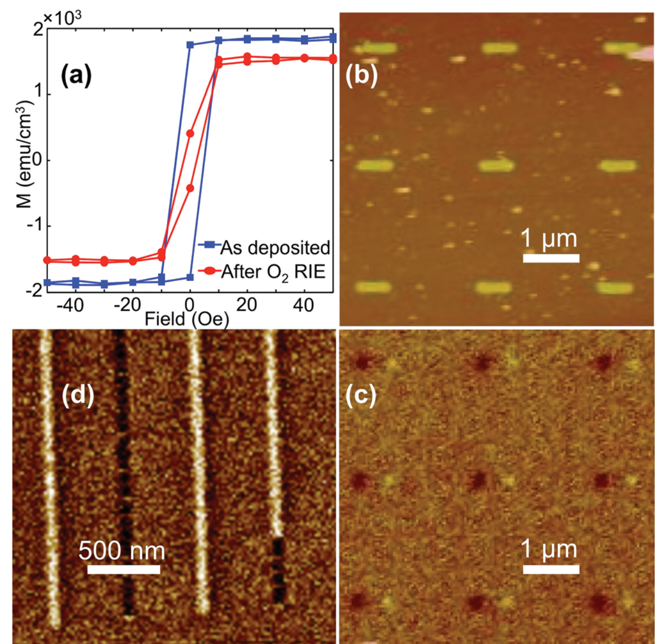

FIG. 5. (Color) (a) Hysteresis loop of unpatterned film with in-plane magnetic anisotropy before and after process flow step 4, showing O_2 RIE slightly reduced the saturation magnetization of the film due to Co oxidation. Blue, square points are as deposited; red, circle points are after the RIE. (b) Atomic force microscope and (c) MFM images of 15 nm thick in-plane anisotropy magnetic bars, showing magnetic dipole contrast. (d) MFM image of the domain structure of a Co/Ni multilayer patterned into lines, showing out of plane magnetic anisotropy. An out of plane demagnetization was applied.

Figure 5 shows data characterizing the magnetic properties of thin films and patterned structures. Figure 5(a) shows the hysteresis loop measured by vibrating sample magnetometry of a continuous 10 nm thick CoFeB thin film with in-plane magnetic anisotropy, before and after process step 4. The 60 s O_2 RIE caused a slight reduction in the saturation magnetization M_s from 1880 emu/cm^3 to 1560 emu/cm^3 due to oxidation of the regions of the film surface exposed to the plasma. But this is still the same order of magnitude of M_s as in the literature,[18] and the parts of the film under the HSQ/PMMA are protected from top–down oxidation.

Figure 5(b) is an atomic force microscope image and (c) is the corresponding magnetic force microscope (MFM) image of an array of bar structures patterned in the CoFeB film. The bars are nominally 600 nm long and 150 nm wide. The alternating dark/light contrast on the bar ends in (c) is indicative of an in-plane magnetic dipole corresponding to each bar as expected from its shape anisotropy; the stray field from the north and south poles is imaged as bright and dark contrast. The small particles between the bars did not produce magnetic contrast, indicating that they were nonmagnetic, weakly magnetic, or superparamagnetic.

Figure 5(d) shows a set of $w=55$ nm lines patterned in the Co/Ni multilayer thin film with perpendicular magnetic

anisotropy.[16] The lines show out of plane "up" and "down" magnetic domains with light or dark contrast, respectively. This indicates that the patterning process preserved the perpendicular anisotropy and hence the multilayer structure of the film.

IV. CONCLUSIONS

This article describes a process for producing thin film metallic wires down to 25 nm width using ion beam etching through a bilayer PMMA/HSQ removable mask. The wires, produced in magnetic films of CoFeB or Co/Ni multilayers, had edge roughness around 2 nm independent of the wire width. This roughness is small compared to domain wall widths (e.g., ∼45 nm in 25 nm wide wires with in-plane magnetic anisotropy).[3] Narrow magnetic wires will be useful for magnetic logic and memory applications, where magnetic domain walls have to propagate long distances driven by low magnetic fields or current densities.

HSQ can resolve sub-10 nm features,[14] so it is likely that this fabrication process can be extended to feature widths below 25 nm. After the high-resolution e-beam lithography patterning and development of the HSQ, the O_2 RIE time would have to be carefully optimized to produce an undercut of the PMMA without removing the PMMA completely.

ACKNOWLEDGMENTS

This work was supported by C-SPIN, one of six STARnet centers of MARCO and DARPA, and by Skolkovo Institute of Technology. The authors gratefully acknowledge Mark Mondol and James Daley of the MIT NanoStructures Laboratory and scanning-electron-beam-lithography facility in the Research Laboratory of Electronics (SEBL at RLE), Sunjae Chung for deposition of the Co/Ni films, and Richard Hobbs for valuable discussions.

[1] S. Bandyopadhyay and M. Cahay, Nanotechnology **20**, 41 (2009).
[2] S. Parkin, M. Hayashi, and L. Thomas, Science **320**, 5873 (2008).
[3] J. A. Currivan, Y. Jang, M. D. Mascaro, M. A. Baldo, and C. A. Ross, IEEE Magn. Lett. **3**, 3000104 (2012).
[4] D. I. Paul, J. Appl. Phys. **53**, 2362 (1982).
[5] H. Tanigawa, T. Koyama, M. Bartkowiak, S. Kasai, K. Kobayashi, T. Ono, and Y. Nakatani, Phys. Rev. Lett. **101**, 20 (2008).
[6] Y. Nakatani, A. Thiaville, and J. Miltat, Nature Mater. **2**, 8 (2003).
[7] H. Yang, A. Jin, Q. Luo, J. Li, C. Gu, and Z. Cui, Microelectron. Eng. **85**, 814 (2008).
[8] M. Rommel and J. Weis, J. Vac. Sci. Technol. B **31**, 6 (2013).
[9] S. Ikeda, J. Hayakawa, Y. Ashizawa, Y. M. Lee, K. Miura, H. Hasegawa, M. Tsunoda, F. Matsukura, and H. Ohno, Appl. Phys. Lett. **93**, 082508 (2008).
[10] I. Nakatani, IEEE Trans. Magn. **32**, 5 (1996).
[11] G. Xiong, D. A. Allwood, M. D. Cooke, and R. P. Cowburn, Appl. Phys. Lett. **79**, 3461 (2001).
[12] Y. S. Jung, J. H. Lee, J. Y. Lee, and C. A. Ross, Nano Lett. **10**, 3722 (2010).
[13] K. Machida, T. Yamamoto, T. Yamaoka, T. Ishibashi, and K. Sato, Jpn. J. Appl. Phys. **45**, L265 (2006).
[14] J. K. W. Yang, B. Cord, H. Duan, K. K. Berggren, J. Klingfus, S. W. Nam, K. B. Kim, and M. J. Rooks, J. Vac. Sci. Technol. B **27**, 2622 (2009).
[15] A. E. Grigorescu and C. W. Hagen, Nanotechnology **20**, 29 (2009).
[16] S. Chung, S. M. Mohseni, V. Fallahi, T. N. Anh Nguyen, N. Benatmane, R. K. Dumas, and J. Åkerman, J. Phys. D: Appl. Phys. **46**, 125004 (2013).
[17] See http://www.lithometrix.com for SUMMIT Litho Image Analysis Software.
[18] D. Wang, C. Nordman, Z. Qian, J. M. Daughton, and J. Myers, J. Appl. Phys. **97**, 10C906 (2005).